Radiation-Induced Degradation of Congo Red Dye over Unsupported and Activated Carbon-Supported Strontium Oxide Nanoparticles

Naz, Falak *+; Imran, Afsha; Ullah, Wajid; Saeed, Khalid; Ali, Sajid; Khan, Muhammad Naeem

Department of Chemistry, Bacha Khan University Charsadda, 24420 Khyber Pakhtunkhwa, PAKISTAN

ABSTRACT: *The textile industry produces a significant amount of liquid effluent pollutants due to the vast amounts of water used in fabric processing. This has resulted in significant water pollution worldwide. The reduction of these dye compounds from industrial wastewater has been achieved using chemical, physical, and biological methods. However, these approaches are time-consuming, costly, and pose disposal problems. Currently, photocatalytic degradation by nanoparticles is attracting significant attention. In this regard, Activated carbon supported and unsupported SrO nanoparticles were synthesized by the wet chemical co-precipitation method. The nanoparticles were characterized by XRD, SEM, EDX, and FT-IR. The Strontium oxide (SrO) and Activated carbon-supported Strontium oxide (Ac/SrO) nanoparticles (NPs) were used as photocatalysts for the photodegradation of Congo red dye in an aqueous medium under UV irradiation. The unsupported SrO and AC/SrO NPs degraded about 93.3% and 97.6% of the dye, respectively, within 100 minutes of irradiation time. The maximum degradation of the dye was achieved at pH 4, 0.06 g of catalyst dose, 15 ppm dye concentration, and a temperature of 45℃ The data were best fitted with pseudo-first-order kinetics. The activity of the recovered catalyst was also examined.*

KEYWORDS: *Nanoparticles; Activated Carbon; Photodegradation; Congo red, Photocatalyst.*

INTRODUCTION

The pollution of water has a great effect on all living organisms because water is a common resource for all ecosystems. Industrialization mainly affects the quality of water and has a very bad effect on all living things. Polluted water has also a bad impact on crops as well as on aquatic plants and animals. Water is mainly polluted by organic dyes, which are produced by industries like fabrics, cosmetics, paper, plastic, leather, ceramic, ink, and food processing [1, 2]. There are a lot of industrial dyes in the world which is unknown, however, financial reports estimated that there is a continuous increase in the number of dyestuffs of over 7×10^5 tons annually [3]. In the textile dyeing process, the selection of dyes is varied concerning fibers. Likewise, wool and nylon fibers are dyed with acid and pre-metalized dyes. Cotton and viscose fibers are dyed with azoic, reactive, direct, pigments, azo, vat, and sulfur dyes [4].

Azo dyes are the most consumed in industry, mainly in textiles, representing up to 35% of dye consumption.

***** *To whom correspondence should be addressed.*
+ *E-mail: falakkaan1@gmail.com*
1021-9986/2022/8/2790-2804 *15/$/6.05*

They are characterized by a structure that contains at least two aromatic compounds linked together by an azo-type chromophore group (-N=N-) [5]. However, the discharge of dyes could cause water pollution problems because of their toxic nature. There are several methods used to discharge these contaminants from water such as conventional methods like adsorption, coagulation, and flocculation; other established methods such as ion exchange, membrane separation, and oxidation; emerging methods such as biodegradation and microbial treatment [6,7], however, one form of waste dye are transferred into another form, thus this type of techniques required further treatment of water [8]. The priority given to photocatalytic degradation by using nanoparticles for wastewater treatment is due to its advantage over the conventional method such as rapid oxidation, no formation of polycyclic products, and oxidation of pollutants [9]. Among these various methods, photocatalysis is considered an eco-friendly cheap, easy, and advanced method for the decolorization of toxic dye [10].

Nanotechnology plays an important role in modern research dealing with the synthesis, design, and manipulation of particle structures which range from approximately 1-100 nm. NanoParticles (NPs) have an extensive range of applications in areas such as health care, cosmetics, food, environmental health, optics, mechanics, biomedical sciences, chemical industries, electronics, space industries, drug-gene delivery, energy science, optoelectronics, catalysis, single electron transistors, light emitters, nonlinear optical devices, and photo-electrochemical applications [11]. Among various nanoparticles metal and metal oxides, nanoparticles exhibit different physicochemical properties and are different than their native bulk compounds in several respects which include surface, optical, thermal, and electrical properties. Metal and metal oxide nanoparticles are synthesized by the addition of oxidizing or reducing/precipitating agents during their synthesis [12].

Various methods are used to synthesize nanoparticles which are mainly categorized into physical and chemical methods. Physical methods involve mechanical milling [13], laser ablation [14], and thermal decomposition in plasma [15]. Chemical methods include sol-gel [16], hydrothermal [17], precipitation [18], combustion [19], etc. The co-precipitation and sol-gel methods are most commonly used for the synthesis of nanoparticles [15]. But in a sol-gel method, the nanoparticles synthesized are amorphous in nature and require further heat treatment for the production of the crystalline particle [20]. Different semiconductors including TiO_2, Fe_2O_3, ZnO, SrO, and CuO [21] and other 2D materials have been reported as photocatalysts for the degradation of pollutants in water. Among several, SrO is an alkaline earth metal oxide, the potential applications, and efficiency of this interesting material were not studied [22]. However, problems associated with their low visible-light harvesting ability and weakness in charge separation have severely limited their applications in environmental remediation [23].

Many types of research have focused on addressing issues through different approaches including growing nanostructures with a large fraction of polar surfaces, alloying with low band gap materials, doping with metals, and inserting carbon allotropes including graphene, Carbon NanoTubes (CNTs), and fullerenes to achieve effective electron transport [24]. Activated carbons are extensively used in many fields due to their high surface area, high porosity, variable functional groups, low ash content, and high mechanical strength [25, 26]. Activated Carbon can develop a topological structure lightly similar to that of graphite, a very well-known semiconductor, in which graphene layers are ordered. This structural order influences the electronic density of AC. If the topological structure of AC becomes lightly similar to that of graphite then the higher electronic conductivity of AC. Having this in mind, it can be suggested a new parameter of correlation between AC properties and photoactivity of SrO. That means, if the electron semiconductivity of AC is good enough (in comparison to graphite) then AC will be able to behave as electron carriers, principally driving out photoelectrons excited by UV-irradiation from SrO conduction band. Concomitantly, this electron carrier's effect contributes to inhibiting the recombination of photogenerated species in semiconductors (h^+ , e^-). This seems to suggest that the higher the electron conductivity of AC the higher photoactivity of SrO [27].

In this work, unsupported and activated carbon-supported Strontium Oxide (SrO) nanoparticles were synthesized by the wet chemical co-precipitation method. The nanoparticles were of low cost with high surface area and can be efficiently used for the degradation of congo red dye.

EXPERIMENTAL SECTION

Chemicals

All the chemicals such as Sr $(NO_3)_2$, Ethanol C_2H_5OH, NaOH, activated carbon having (purity ≥ 99.9%), and Nitric acid (HNO_3) were purchased from Sigma-Aldrich, while Congo red dye ($C_{32}H_{22}N_6Na_2O_6S_2$) having purity ≥98% was purchased from Merck chemical company. All the above chemicals were of analytical grade and were utilized as received.

Synthesis of unsupported and activated carbon Strontium oxide NPs

100 mL Strontium nitrate Sr $(NO_3)_2$ salt (0.1 M) solution was taken in a beaker and (0.2 M) NaOH solution was added dropwise until the pH became basic. The mixture was stirred continuously for 2 h at 80 °C and was then cooled to obtain the precipitate. The precipitate was separated by filtration, followed by washing several times with deionized water and ethanol. The precipitate was dried in an oven at 100 °C and calcined in a furnace at 500°C for 2 h to obtain the SrO NPs.

For the Synthesis of AC/SrO NPs 100 mL, Sr $(NO_3)_2$ salt (0.1 M) solution, and 1g activated carbon were mixed, and then (0.2M) solution of NaOH was added into it dropwise until a basic pH was obtained. The mixture was stirred continuously for 2 h at 80 °C and was then cooled to obtain the precipitate. The precipitate was separated by filtration, followed by washing several times with deionized water and ethanol. The precipitate was dried in an oven at 100 °C and calcined in the furnace at 500°C for 2 h to obtain the AC/SrO NPs.

Photocatalytic degradation of Congo red dye by using supported and unsupported SrO NPs

The supported and Unsupported SrO were used for the photocatalytic degradation of Congo Red dye under UV light (15W UV lamp). The point of zero charges of the catalysts was determined by plotting the initial pH (4-10) of the solution versus the change in pH (after the addition of the catalyst and stirring for 24h). The experiments were carried out at a pH lower than the PZC. The solution was first kept in dark for 20 minutes to maintain the adsorption-desorption equilibrium. After this, the solution was kept under UV light, and the effect of irradiation time, the concentration of dye, temperature, catalyst dose, and pH on the degradation of Congo red dye was studied. The sample was taken every 20 min and analyzed *via* a UV-Visible spectrophotometer. The percent degradation was calculated by using the following equation:

$$\text{Degradation (\%)} = \frac{\text{Co} - \text{C}}{\text{Co}} \times 100 \quad (1)$$

$$\text{Degradation (\%)} = \left(\frac{\text{A}_0 - \text{A}}{\text{A}_0}\right) \times 100 \quad (2)$$

Where C_o represents the initial dye concentration, C is the dye concentration after UV light illumination, A_o is the initial absorbance and A is the dye absorbance after time t.

Instrument

The morphological study was carried out by SEM (Model No. JEOL-Jsm-5910, JEOL Company, Japan). The XRD analysis was performed by an X-ray diffractometer (Model JEOL-300). The elemental composition of the sample was studied by EDX spectrometer (Model Inea 200, UK, company Oxford). The FT-IR analysis was carried out via FT-IR (PerkinElmer) spectrometer. The concentration of dye was analyzed via UV-Visible Spectrophotometer (Shimadzu 160 A, Japan).

RESULTS AND DISCUSSION

X-Ray Diffraction (XRD) analysis

The XRD pattern of AC-supported and unsupported SrO NPs is presented in Fig. 1. The strong and sharp peaks that are present show the crystalline structure and purity of SrO nanoparticles. The diffraction peaks at 2θ values 26.85°, 36.74°, 41.95°, and 52.40° are assigned to (111), (130), (220), and (222) planes of SrO, respectively. The XRD spectra of both supported and unsupported SrO NPs is similar to that of a previously reported XRD pattern of SrO synthesized via the sol-gel method [28].

Scanning Electron Microscopy (SEM)

The morphological study of the nanoparticles was done by scanning electron microscopy. Fig. 2(a, b) shows the SEM images of prepared SrO and AC/SrO nanoparticles. The SEM images show that the unsupported SrO is in aggregated form, while AC/SrO nanoparticles appeared in well-dispersed form, thus in the latter case, a large amount of SrO will be exposed on the surface of the carbon. As a result, the active site available on the surface of carbon will increase. This may also contribute to the high photocatalytic activity of AC/SrO nanoparticles than unsupported SrO.

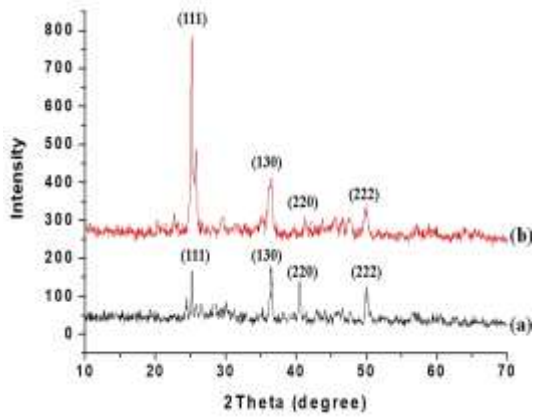

Fig. 1: XRD (a) unsupported SrO and (b) AC/SrO nanoparticles.

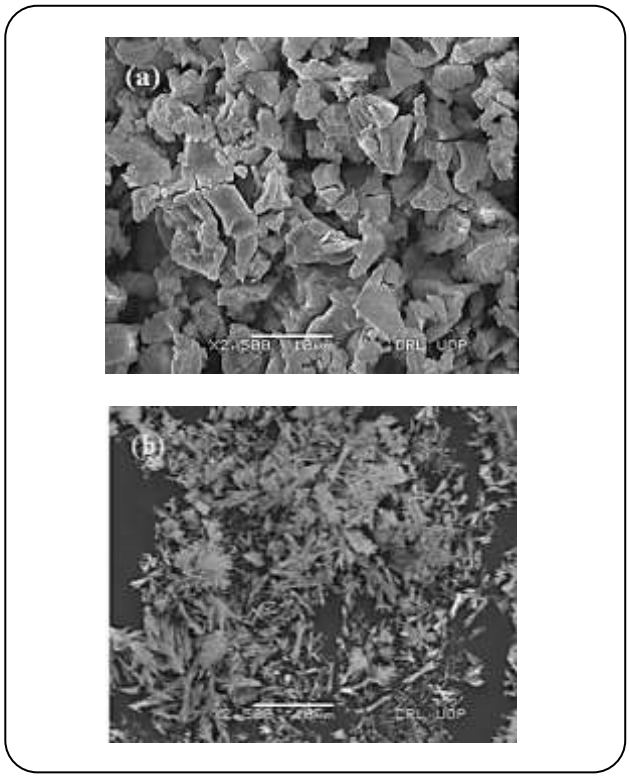

Fig. 2: SEM images of (a) unsupported SrO and (b) AC/SrO nanoparticles.

Energy Dispersive X-Ray (EDX)

The elemental composition of SrO and AC/SrO was confirmed from the EDX analysis of the nanoparticles. Fig. 3 shows EDX spectra of SrO and AC/SrO nanoparticles. Figure 1(a) shows that oxygen is present with a weight percent of 23.96%, while Sr is present at 76.04%. Figure 3(b) shows that Carbon is present in weight percent of 10.94%, oxygen is present at 25.63%, and strontium is 55.05%. The EDX analysis shown in Fig. 3, indicates the existence of certain elements, such as Mg, Ca, Fe, Ba, which are constituents of mineral compositions of the activated carbon used.

Fourier Transform InfraRed (FT-IR) spectroscopy

Fig. 4 shows the FTIR spectra of SrO and AC/SrO NPs. Generally, the stretching vibrations of Sr-O have been detected between 400-900 cm^{-1} [29]. The peak observed at 597-810 cm^{-1} was assigned to the vibration of the Sr-O-Sr bond in SrO lattice. Peaks observed at 1402 cm^{-1} were ascribed to C-O and C-H stretching vibrations. A small peak has been detected between 3000-3200 cm^{-1} which is assigned to the OH stretching. In Fig. 4(b) the maximum absorption at 1402 cm^{-1} is due to the presence of activated carbon in the SrO NPs [30].

Band gap

Fig. 5 shows the band gap energy (Eg) for SrO and AC/SrO calculated from the UV-visible spectra. The optical band gap energy (Eg), was calculated from the linear part of the plots between $(\alpha \times h\upsilon)^2$ and photon energy ($h\upsilon$). The Eg calculated for unsupported SrO was 3.5eV, while in the case of AC/SrO it decreases to 3.3eV. Similarly, Mohammed M. Rahman synthesized SrO_2 and CNT-supported SrO_2 NPs in which their band gap decreased with the support of CNT [31].

Point of Zero Charge (PZC) and effect of pH

To calculate the Point of Zero Charge (PZC) of the catalyst about 18 mg catalyst was added to 0.1M Sodium nitrate solution taken in seven separate flasks. The pH of the solution was adjusted from 4-10 by the addition of 0.1M acid or 0.1M base. The solution was stirred on a magnetic stirrer for 24 hours and was then filtered and its pH was measured. The PZC was calculated by plotting pH versus change in pH (ΔpH) and was found to be 5 as shown in Fig. 6.

Kinetics study

The pure and AC/SrO_2 photocatalytic degradation of Congo red dye was described by Eley–Rideal (E-R) mechanism process, one of the mechanisms used for heteronomous catalytic processes. This mechanism indicates that one reactant adsorbed in fluid form while the other reacts in adsorbed phase [32-34].

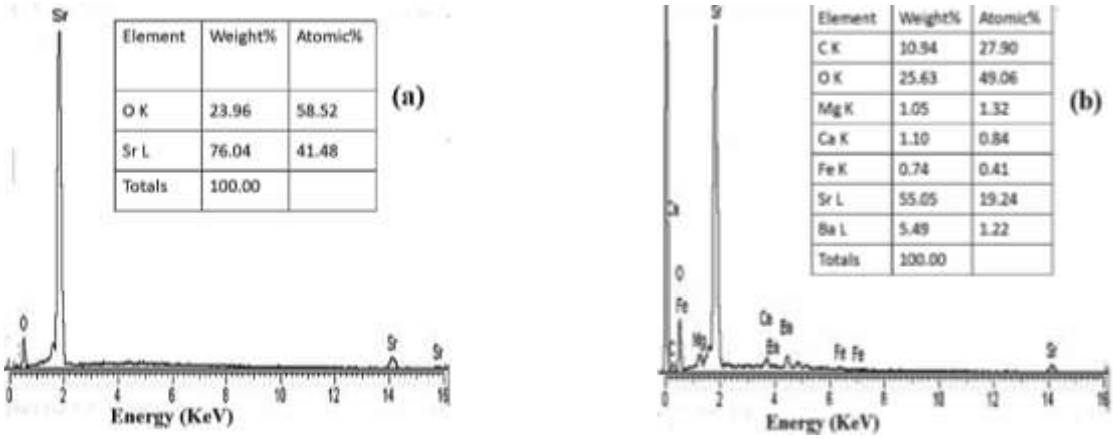

Fig. 3: EDX spectra of (a) SrO and (b) AC/SrO nanoparticles.

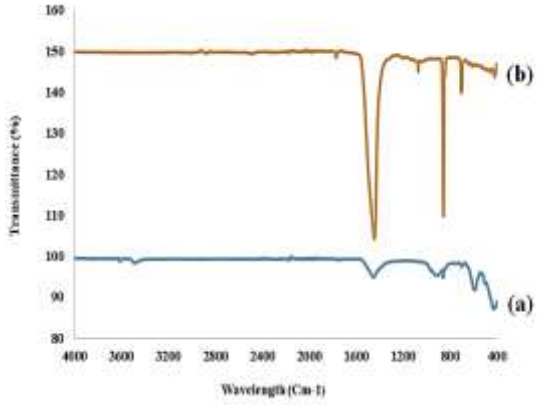

Fig. 4: FT-IR Spectra (a) SrO and (b) AC/SrO nanoparticles.

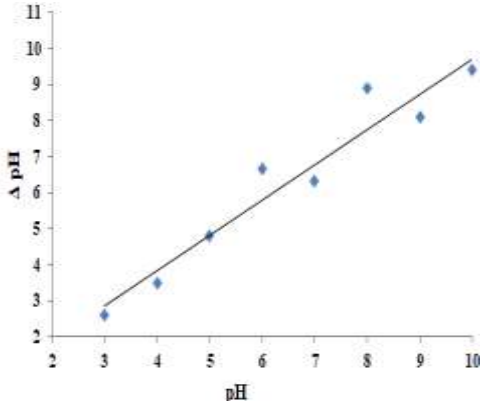

Fig. 6: Determination of PZC of the photocatalyst.

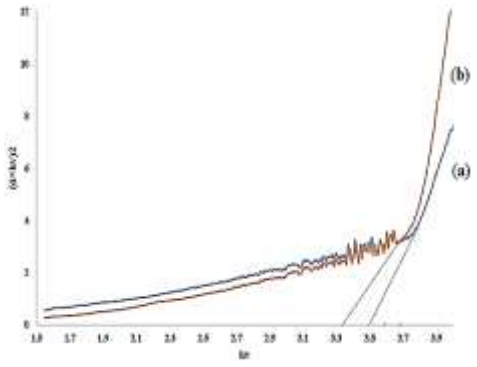

Fig. 5: Band gap of (a) SrO and (b) AC/SrO nanoparticles.

Following the equation used to understand the E-R mechanism.

$$-\frac{\mathrm{d}\,(Co)}{\mathrm{dt}} = \mathrm{Kr\ O2\ (ads)\ (Co)n} \qquad (3)$$

Where *Kr* represents the rate constant of the reaction and O_2 (ads) represents adsorb oxygen at the catalyst surface.

By taking the O_2 constant we obtained,

$$\frac{-d(Co)}{dt} = \mathrm{K\ (Co)n} \qquad (4)$$

By converting them into the pseudo-first-order reaction (n = 1), the kinetic Eq. (4) changes to kinetics Eq. (5) which is a pseudo-first-order kinetics model as suggested by other researchers as well [35-38].

$$\frac{\ln(\mathrm{Co})\mathrm{o}}{(\mathrm{Co})\mathrm{t}} = \mathrm{K1.t} \qquad (5)$$

Similarly, by applying pseudo-second-order kinetics to the degradation of dye, the equation used is,

$$\frac{1}{(\mathrm{Co})\mathrm{t}} = \mathrm{K2\ .t} + \frac{1}{(\mathrm{Co})\mathrm{o}} \qquad (6)$$

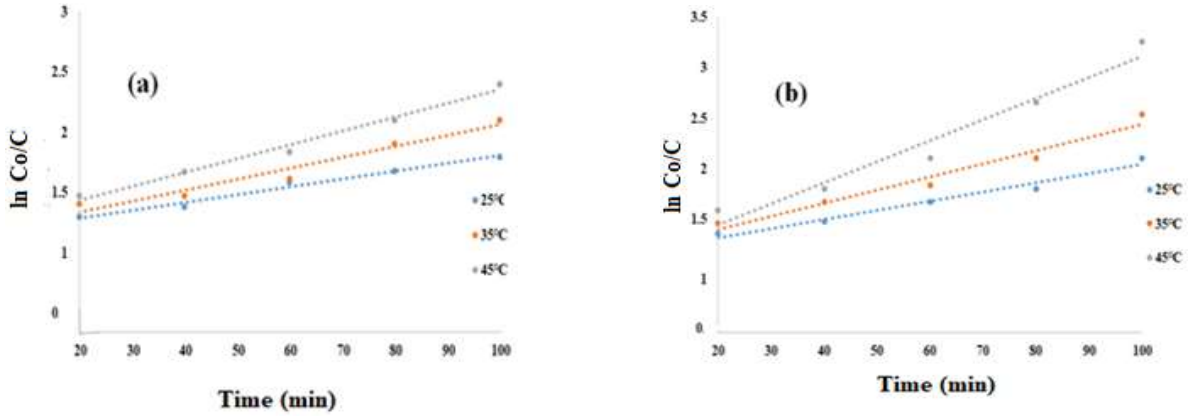

Fig. 7: Pseudo first order kinetics for degradation of dye on (a) unsupported SrO and (b) AC/SrO NPs at different temperatures.

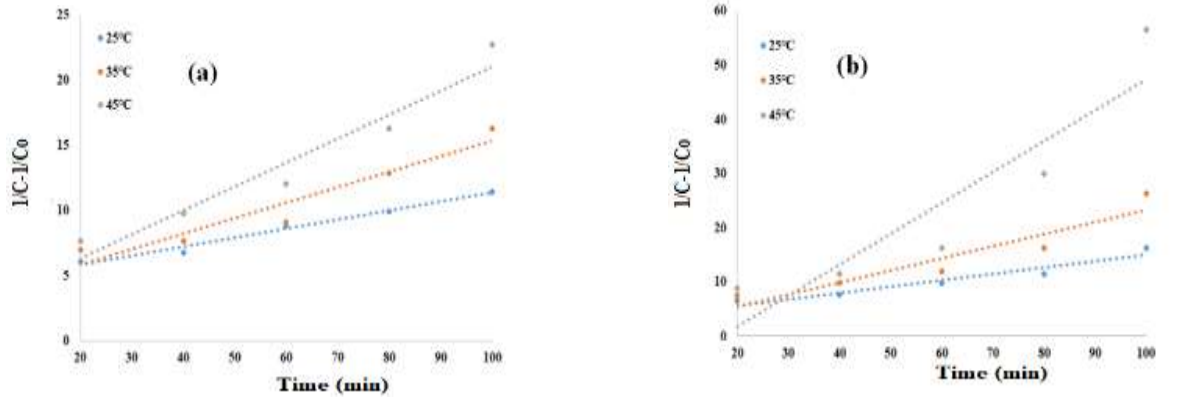

Fig. 8: Pseudo-second-order kinetics for degradation of dye on (a) unsupported SrO and (b) AC/SrO NPs at different temperatures.

Equation (4) can be written in a more simplified form as

$$\frac{1}{(\mathrm{Co})\mathrm{t}} - \frac{1}{(\mathrm{Co})\mathrm{o}} = \mathrm{K2}\,.\,\mathrm{t} \qquad (7)$$

Where $(C_0)^t$ and $(C_0)^o$ represent the final and initial concentration of the dye, respectively.

Equations (5) and (7) were applied to the degradation of dye at different temperatures.

Both the pseudo-first and pseudo-second-order kinetics were applied to the degradation of dye at different temperatures as shown in Figs. 7 and 8, respectively.

The apparent rate constants (K_1 and K_2) and correlation coefficient were calculated from the slope of Figs. 6 and 7 and are shown in table 1. As the R^2 values obtained were highest in pseudo-first-order reaction both for supported SrO and SrO, therefore, the data were best fitted to pseudo-first-order kinetics, the same results are also reported previously [39].

The activation energy of the reaction was calculated by applying the Arrhenius equation, the graph was plotted between ln k Vs 1/T. From the slope of the graph (Fig. 9) the activation energy was calculated to be 38.1kJ/mol and 62.35kJ/mol for AC/SrO_2 and SrO_2 respectively as shown in Table 1.

Similarly, pseudo-first and pseudo-second-order kinetics were also applied to the dye degradation at different initial concentrations of the dye as shown in Figs. 10 and 11 respectively.

From the slope of Figs. 10 and 11, the apparent rate constant (K_1 and K_2) and correlation coefficient values were calculated at the different initial concentrations of dye and are shown in Table 2.

The above kinetics investigation exhibits that supporting SrO_2 nanoparticles on AC increases the rate of degradation of Congo red dye. The greater R^2 value for pseudo-first-order kinetics in dye concentrations and temperatures study exhibited that the data is best fitted to pseudo-first-order kinetics [40].

Table 1: Kinetic constant parameter values for the photocatalytic degradation of dye at different temperature.

Temperature(°C)		Pseudo-first-order kinetics		Pseudo-second-order kinetics		Activation Energy (KJ/mol)
		K_1	R^2	K_2	R^2	
Unsupported SrO	25	0.0065	0.9799	0.0696	0.9825	62.35
	35	0.0091	0.9526	0.1188	0.9227	
	45	0.0114	0.9865	0.1833	0.9397	
AC/SrO	25	0.0091	0.973	0.1165	0.9276	38.1
	35	0.0129	0.9647	0.221	0.8856	
	45	0.0209	0.957	0.5699	0.8428	

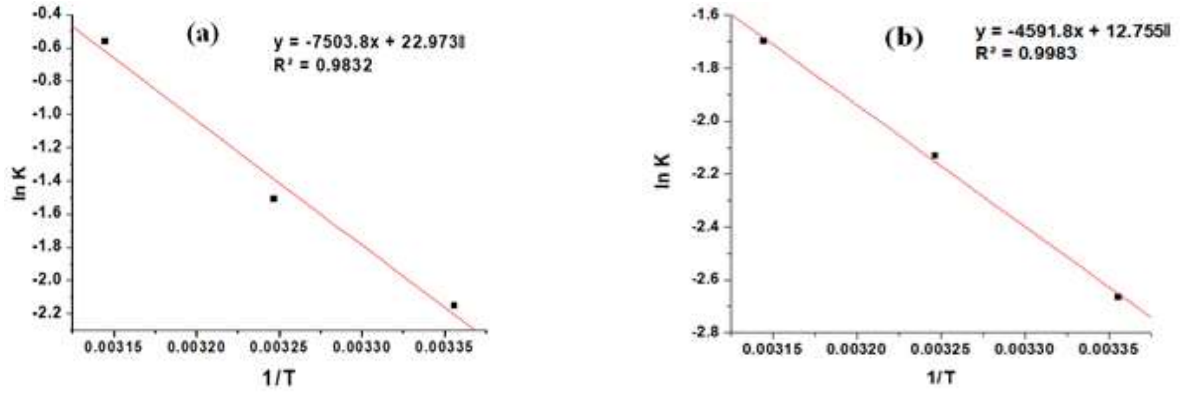

Fig. 9: Application of Arrhenius equation to the degradation of dye on (a) unsupported SrO and (b) AC/SrO NPs.

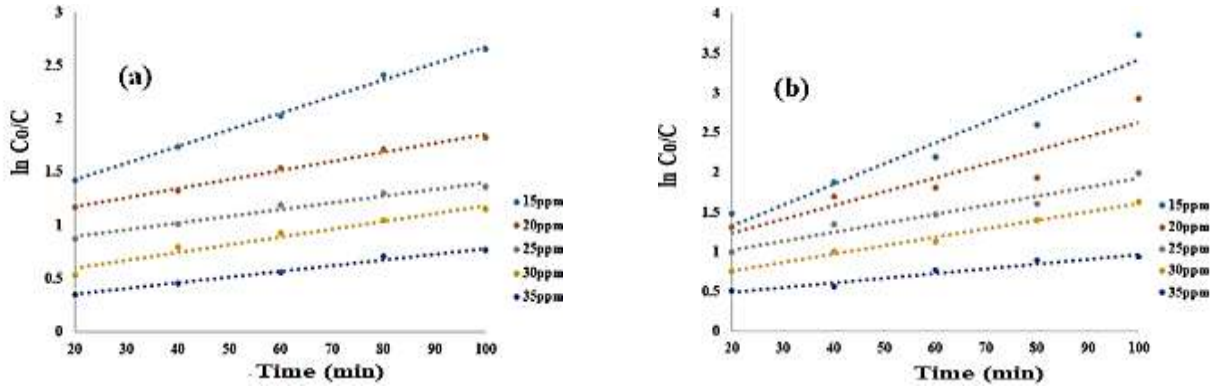

Fig. 10: Pseudo first-order kinetics for degradation of dye on (a) unsupported SrO and (b) AC/SrO NPs at different concentrations of the dye.

Photocatalytic degradation mechanism

Valence band holes (VBh^+) and conduction band electrons (CBe^-) are generated when aqueous SrO suspension is irradiated with UV-visible light energy greater than its band-gap energy (Eg=3.59eV). These electron-hole pairs interact separately with other molecules. Valence band holes (VBh+) react with surface-bound H_2O or OH to produce hydroxyl radical ($OH^{\cdot}$). Valence band holes can also oxidize organic molecules. Conduction Band electrons (CBe^-) reduce molecular oxygen to generate

Table 2: Kinetic constant parameter values for the photocatalytic degradation of dye at different initial concentrations of the dye.

Concentration (ppm)		Pseudo-first-order kinetics		Pseudo-second-order kinetics	
		K_1	R^2	K_2	R^2
Unsupported SrO	15	0.0157	0.997	0.2567	0.971
	20	0.0085	0.9925	0.0619	0.9951
	25	0.0064	0.9737	0.0259	0.9863
	30	0.0074	0.9575	0.0184	0.9868
	35	0.0055	0.9899	0.0098	0.9884
AC/SrO	15	0.0262	0.9198	0.8158	0.7117
	20	0.0174	0.8305	0.2548	0.6848
	25	0.0113	0.957	0.0696	0.9143
	30	0.0106	0.9887	0.0346	0.9646
	35	0.0059	0.9506	0.0113	0.9575

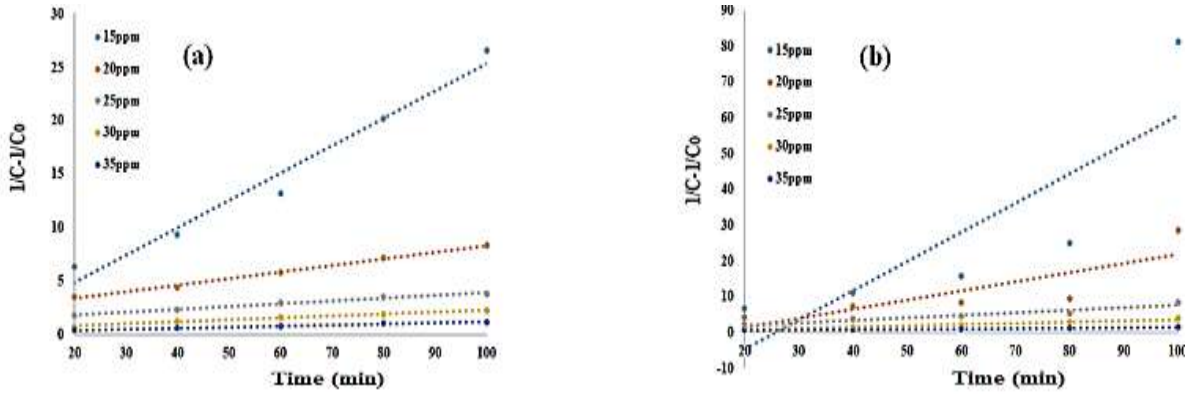

Fig. 11: Pseudo second-order kinetics for degradation of dye on (a) unsupported SrO and (b) AC/SrO NPs at different concentrations of the dye.

superoxide radicals [41]. Scheme 1 represents the possible degradation mechanism of Congo red dye.

$$SrO + h\upsilon_{(UV)} \longrightarrow SrO\left(VBh^{+}\right) + \left(CB\ e^{-}\right) \quad (8)$$

$$SrO\left(VBh^{+}\right) + H_2O \longrightarrow SrO + H^{+} + OH \quad (9)$$

$$SrO\left(VBh^{+}\right) + OH^{-} \longrightarrow SrO + OH^{\cdot} \quad (10)$$

$$SrO\left(CBe^{-}\right) + O_2 \longrightarrow SrO + O_2^{-} \quad (11)$$

$$\text{Congo Red} + OH^{\cdot} \longrightarrow \text{Degradable product} \quad (12)$$

$$\text{Congo Red} + O_2^{-} \longrightarrow \text{Degradable product} \quad (13)$$

Effect of temperature

The photocatalytic degradation of dye was also carried out at different temperatures i-e 25, 35, and 45 ^{o}C while keeping all the other parameters constant. Fig. 12 shows that the degradation efficiency increased with the increase in temperature and the maximum degradation of 90.9% was observed at 45 ^{o}C in the unsupported catalyst, while in the supported catalyst the maximum degradation efficiency was 96.15%. This is due to the fact that the surface activity is not high so an increase in temperature exerts an insignificant impact on the chemical reactions and enhances the degradation process in general by decreasing the activation energy [42].

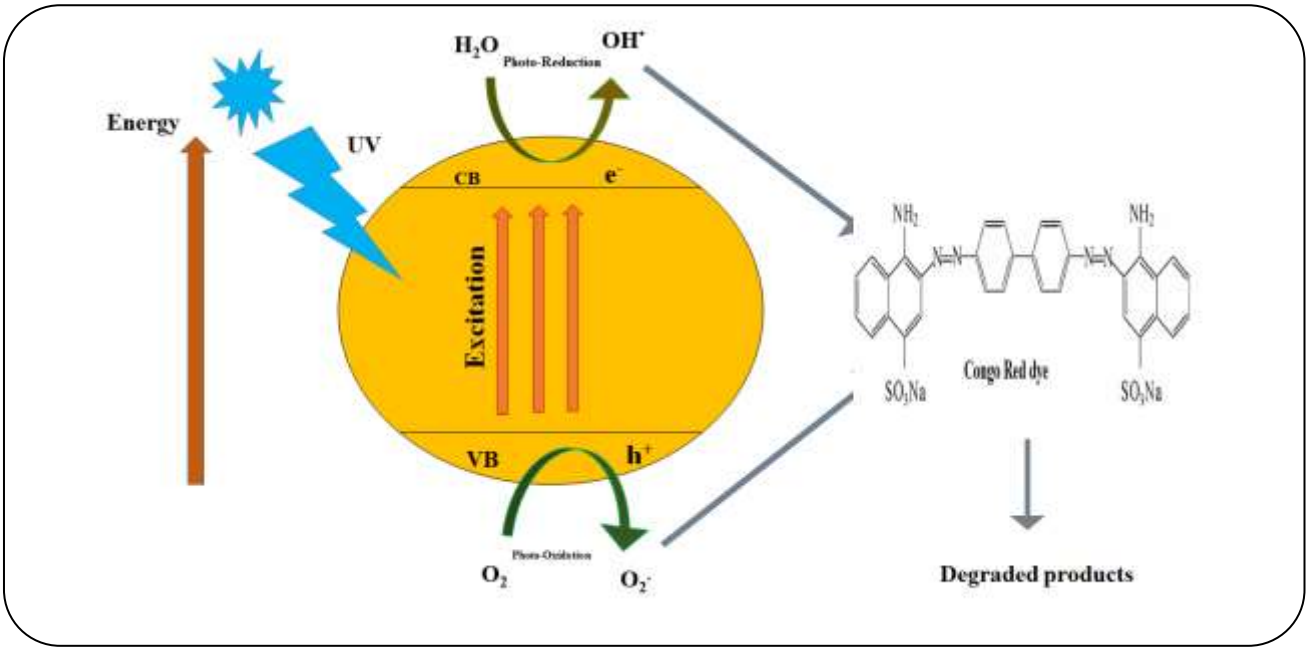

Scheme 1: Photocatalytic degradation mechanism of Congo red dye.

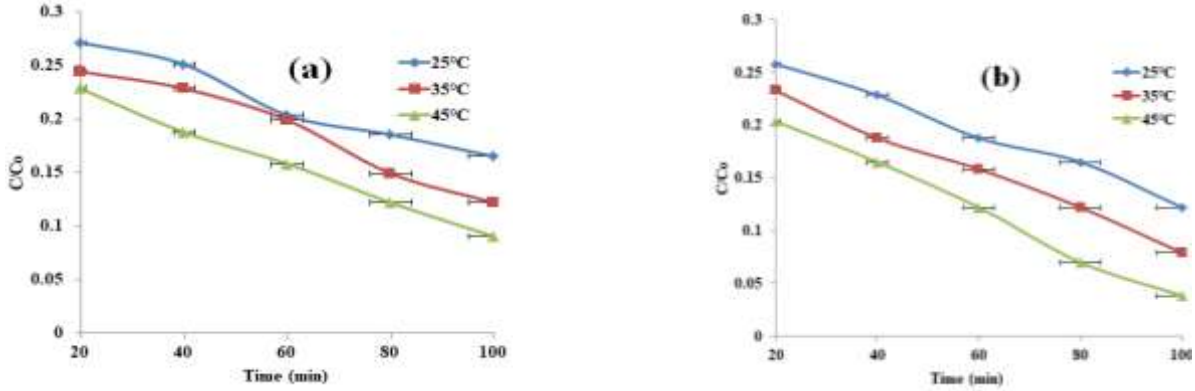

Fig. 12: Effect of temperature on degradation of dye on (a) unsupported SrO and (b) AC/SrO NPs.

Effect of dye initial concentration

The Congo red degradation was studied at the different initial concentrations of dye i-e (15, 20, 25, 30, and 35) ppm while keeping all the other parameters kept constant like catalyst dose, pH, and temperature (Fig. 13). The catalyst was very effective towards the degradation of dye and degraded 15ppm dye in initial 20 minutes with 74.3% degradation efficiency in unsupported catalyst, while in AC/SrO it degraded 77.2% of the dye was in 20 minutes. The maximum degradation observed was 93.3% in time intervals 100 minutes for unsupported catalysts, while in AC/SrO catalyst the maximum degradation in 100 min was 97.6%. On increasing the concentration of dye the degradation efficiency of dye decreases. It is because as the number of dye molecules increases, the amount of light (quantum of photons) penetrating inside the dye solution to reach the catalyst surface is reduced due to the hindrance in the path of light. Therefore the formation of the reactive hydroxyl and superoxide radicals is also reduced simultaneously [43]. On the other hand, at higher concentrations, a lower % of degradation has been observed due to the saturation of the active adsorption sites [44]. The Congo red degradation study was also performed by *Supriya S* and *Sathish S* (2020) at which the maximum degradation observed was 83.4%. From their study, it was observed that the percentage of decolorization

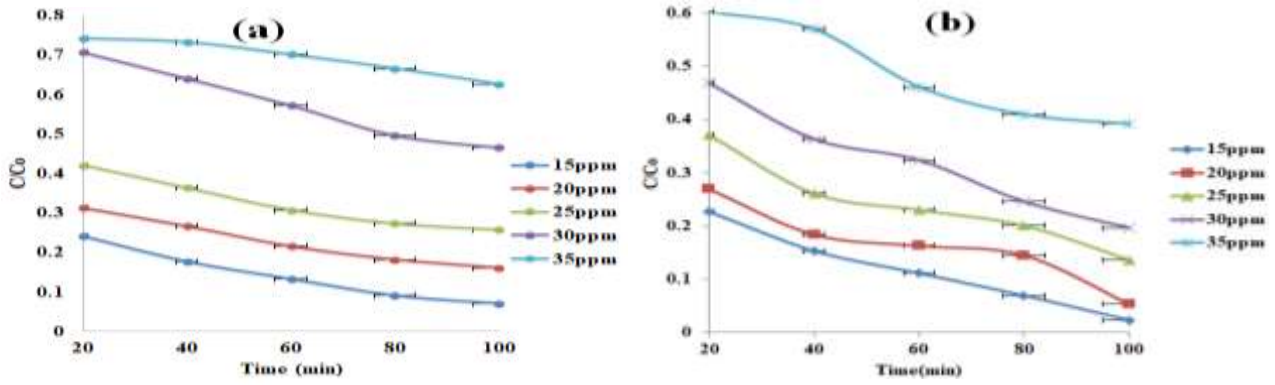

Fig. 13: Effect of concentration of dye on degradation efficiency using (a) unsupported SrO and (b) AC/SrO nanoparticles.

decreased from 83.4% to 40.6% with the increase in the initial concentration of the dye solution from 0.4–1.2 x 10-4 M. The high decolorization efficiency for lower dye concentrations is due to the efficient generation of hydroxyl radicals and their high probability of interaction with the dye molecules. When Congo red dye concentration increases, the probability of interaction of the radical species with the dye molecules decreases and thereby decreases the decolorization efficiency. This decrease is due to the presence of a large number of dye molecules available for adsorption compared to the number of active sites present on the surface of the nanoparticles. High initial dye concentration also competes with the adsorption process of the oxidizing agents on the surface of the catalyst and decreases the formation of active radical species such as $O2^{\bullet-}$ and $OH^{\bullet}$, which are the main oxidants in the decolorization process [45].

Effect of Catalyst dosage

Fig. 14 shows the effect of catalyst dose on the degradation of dye by changing the amount of catalyst (0.02g, 0.04g, 0.06g, 0.08g, 0.1g) for both SrO and AC/SrO while keeping all the other parameters constant i.e. temperature, pH, the concentration of dye. It was found that the photodegradation of dye increased with the increase in dose up to 0.06g. The maximum degradation efficiency was 76.8% in unsupported SrO, while in AC/SrO catalyst, the maximum degradation efficiency was 83.4 %. The photodegradation of dye increases with increasing catalyst dosage up to 0.06g, which is the feature of heterogeneous photocatalysis. The increase in catalyst amount actually increases the number of active sites on the catalyst surface thus causing an increase in the formation of many·OH radicals can take part in the decolorization of dye solution. Further increase in catalyst amount beyond the optimum limit (0.06g) makes the solution turbid and thus blocks UV light radiation for the reaction to proceed and therefore percentage degradation starts decreasing [46].

Effect of pH

Fig. 15 shows the effect of pH on the degradation of Congo red by varying the pH from 4 to 10 while keeping all other parameters constant. It was observed that the degradation of dye decreased with an increase in pH and the maximum degradation observed at pH 4 in pure SrO was 77% while in AC/SrO the maximum degradation at pH 4 was 83.1%. The degradation efficiency of dyes on photocatalyst is significantly dependent on the PZC of the photocatalyst surface and the nature of the dye (cationic, anionic, or neutral). The photocatalyst surface is positively charged when pH < PZC, and therefore the anionic dyes like CR, electrostatic attractions result in dye adsorption and enhance the degradation efficiency of CR, while the surface of photocatalyst is negatively charged when pH > PZC, followed by the enhancement of electrostatic repulsion, resulting in the decrease degradation efficiency of CR [47]. Another reason for the behavior of acidic pH is the formation of hydrogen bonds between the sulfonate or amine sites of dye molecules and the photocatalyst's hydroxyl groups. An increase in the pH of the dye solution, give rise to a decrease in adsorption. Generally, the anionic sites of the dye compete with the anion $OH^{\bullet}$ at higher pHs, which are adsorbed onto positive charges of the photocatalyst. This leads to the blocking of activated sites [48].

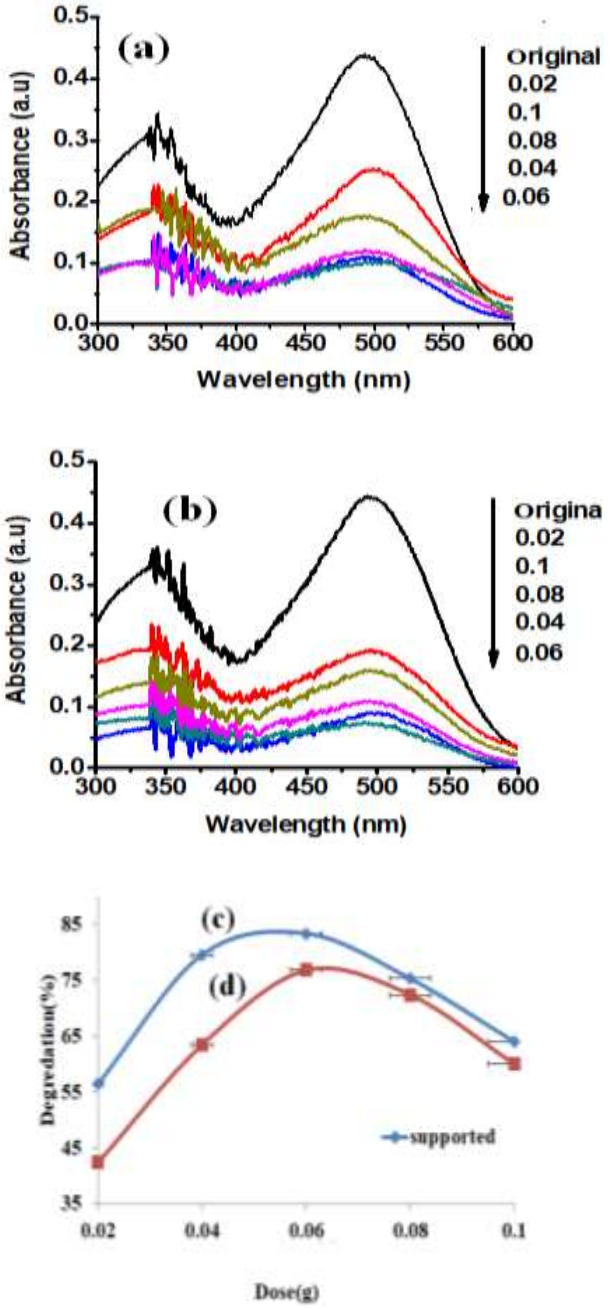

Fig. 14: Absorption spectra for the effect of catalyst dose on dye degradation on (a) unsupported SrO, (b) AC/SrO, (c) percent degradation of dye on AC/SrO, and (d) percent degradation of dye on unsupported SrO at different catalyst dose.

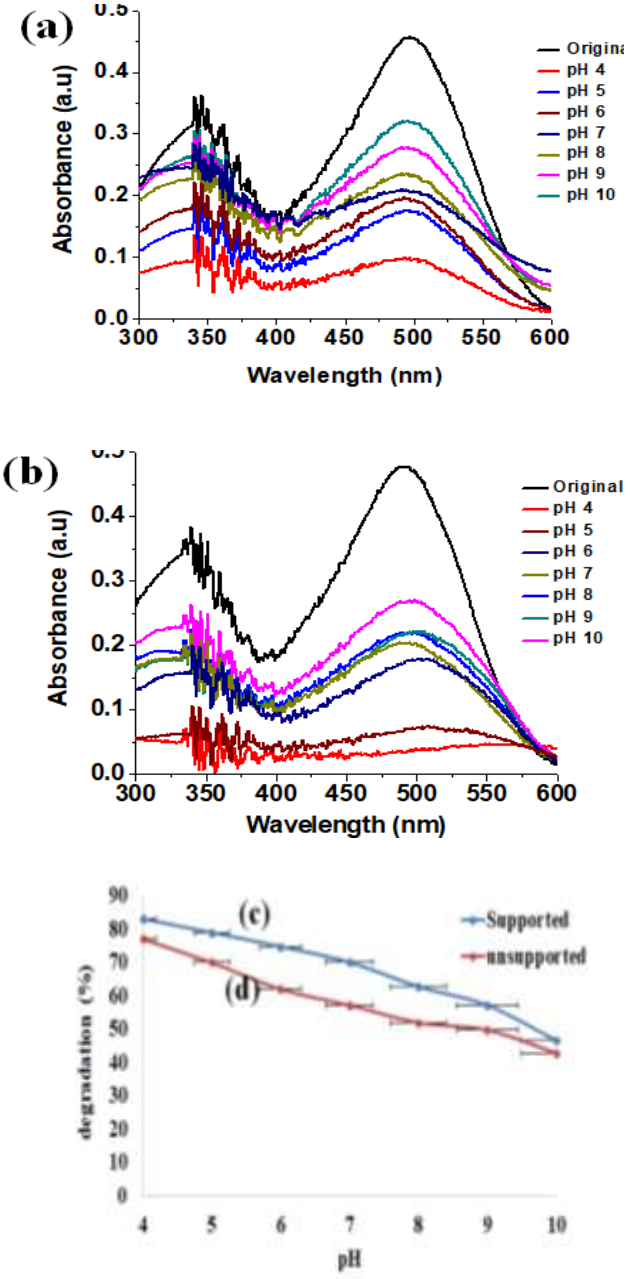

Fig. 15: Absorption spectra for the effect of pH on degradation of dye on (a) unsupported SrO and (b) AC/SrO NPs, (c) percent degradation of dye on AC/SrO, and (d) percent degradation of dye on unsupported SrO at different pH.

Recyclability of catalyst

The photocatalyst and Congo red mixture were agitated and illuminated with UV light and after desired time, the mixture was centrifuged to remove the photocatalyst. The obtained photocatalyst was washed several times with double distilled water and kept in an oven for 12h at 80 °C and reused for the degradation of Congo red dye. The photodegradation of Congo red by the recycled photocatalysts is shown in Fig. 16. It was observed that the recycled Pure SrO degraded 65.5% dye, while the recycled AC/SrO degraded 72.2% of the dye in 100 minutes. The difference of decrease in the percentage from the original the catalyst was

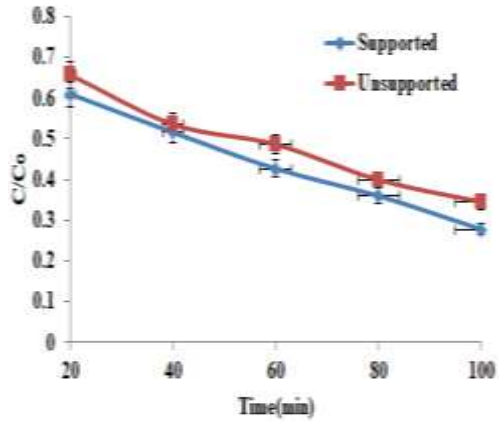

Fig. 16: Degradation of Congo red dye using recycled photocatalysts.

25.4% in AC/SrO and 27.8% in SrO. The result shows that the recycled photocatalysts' efficiency was decreased due to three reasons 1, due to the loss of some active sites and decreased collection efficiency of photons [49]. 2, The adsorptive catalytic surface activity of the catalyst gradually decreased because of the obstruction of the pores and the active sites by catechol and its intermediates after each cycle [50]. The properties of magnetic nanoparticles, such as aggregation (this effect can reduce the effective surface area and decrease the number of active sites) and fouling, might change during the seven cycles [51].

CONCLUSIONS

The SrO and AC/SrO NPs were synthesized through the co-precipitation technique. The photocatalytic degradation of Congo red dye was carried out on the as-synthesized NPs under UV light irradiation. The results revealed that the photocatalytic activity of SrO has been significantly improved by supporting it with Activated carbon. The optimum condition for the photocatalytic degradation of dye was obtained at a dye initial concentration 15ppm, catalyst dose 0.06 g, pH 10, and a temperature of 45 ℃. The dye degradation efficiency increased with the increase in temperature and catalyst dose while it decreased with the increase in dye initial concentration and pH. The data were best fitted with pseudo-first-order kinetics.

Received : Jan. 12, 2021 ; Accepted : Dec. 6, 2021

REFERENCES

[1] Zheng B., Guo Q., Wei Y., Deng H., Ma K., Liu J., Zhao Y., Water Source Protection and Industrial Development in the Shandong Peninsula, China from 1995 to 2004: A Case Study, *Resour. Consev. Recy.*, **52(8-9)**: 1065-1076 (2008).

[2] Nirmaladevi S., Palanisamy P.N., A Comparative Study of the Removal of Cationic and Anionic Dyes from Aqueous Solutions Using Biochar as an Adsorbent, *Desalination Water Treat.*, **175**: 282-292 (2020).

[3] Pandey N., Shukla S.K., Singh N.B., Water Purification by Polymer Nanocomposites: An Overview, *Nanocomposites.*, **3(2)**: 47-66 (2017).

[4] Sakthisharmila P., Palanisamy P.N., Manikandan P., Operational Cost Analysis for the Treatment of Various Textile Effluents by Electrochemical Process Using Stainless Steel and Aluminum Electrodes, *Iran. J. Chem. Chem. Eng. (IJCCE)*, **38(5)**: 165 - 173 (2019).

[5] Mezohegyi G., van der Zee F. P., Font J, Fortuny A., Fabregat A., Towards Advanced Aqueous Dye Removal Processes: A Short Review on the Versatile Role of Activated Carbon, *J. Environ. Manage.*, **102:** 148-164 (2012).

[6] Arslan-Alaton I., Ferry J.L., Application of Polyoxotungstates as Environmental Catalysts: Wet Air Oxidation of Acid Dye Orange II, *Dyes. Pigments.*, **54(1)**: 25-36 (2002).

[7] Sakthisharmila P.N.P.P., Palanisamy P.N., Manikandan P., Removal of Benzidine Based Textile Dye Using Different Metal Hydroxides Generated in Situ Electrochemical Treatment-A Comparative Study, *J. Clean. Prod.*, **172:** 2206-2215 (2018).

[8] Sobana N., Muruganadham M., Swaminathan M., Nano-Ag Particles Doped TiO_2 for Efficient Photodegradation of Direct Azo Dyes, *J. Mol. Catal. A Chem.*, **258(1-2)**: 124-132 (2006).

[9] Vickers N.J., Animal Communication: When I'm Calling You, Will You Answer Too, *Curr. Biol.*, **27(14)**: 713-715 (2017).

[10] Colvin V. L., Schlamp M. C., Alivisatos A. P., Light-Emitting Diodes Made from Cadmium Selenide Nano Crystals and a Semiconducting Polymer, *Nature.*, **370(6488)**: 354-357 (1994).

[11] Sanchez-Dominguez M., Boutonnet M., Solans C., A Novel Approach to Metal and Metal Oxide Nanoparticle Synthesis: the Oil-in-Water Microemulsion Reaction Method, *J. Nanopart. Res.*, **11(7)**: 1823-1828 (2009).

[12] Bodaghi M., Mirhabibi A., Tahriri M., Zolfonoon H., Karimi M., Mechanochemical Assisted Synthesis and Powder Characteristics of Nanostructure Ceramic of α-Al2O3 at Room Temperature, *Mater. Sci. Eng B.*, **162(3)**: 155-161 (2009).

[13] Johnston G.P., Muenchausen R., Smith D.M., Fahrenholtz W., Foltyn, S., Reactive Laser Ablation Synthesis of Nanosize Alumina Powder, *J. Am. Ceram. Soc.*, **75(12)**: 3293-3298 (1992).

[14] Rajaeiyan A., Bagheri-Mohagheghi M. M., Comparison of Sol-Gel and Co-Precipitation Methods on the Structural Properties and Phase Transformation of γ and α-Al_2O_3 Nanoparticles, *Adv. Manuf.*, **1(2)**: 176-182 (2013).

[15] Nguefack M., Popa A.F., Rossignol S., Kappenstein C., Preparation of Alumina Through a Sol-Gel Process. Synthesis, Characterization, Thermal Evolution and Model of Intermediate Boehmite, *Phys. Chem. Chem. Phys.*, **5(19)**: 4279-4289 (2003).

[16] Mishra D., Anand S., Panda R. K., Das R. P., Hydrothermal Preparation and Characterization of Boehmites, *Mater. Lett.*, **42(1-2)**: 38-45 (2000).

[17] Rahmanpour O., Shariati A., Nikou M. R. K., New Method for Synthesis Nano Size [gamma]-A l_2O_3 Catalyst for Dehydration of Methanol to Dimethyl Ether, *Int. J. Chem. Eng.*, **3(2)**: 125-132 (2012).

[18] Zhai X., Fu Y., Chu G., New Technology Reports Combustion Synthesis of the Nano/Structured Alumina Powder, *Nanoscience.*, **11(4)**: 286-292 (2006).

[19] Saeed K., Khan I., Park S. Y., TiO2/Amidoxime-Modified Polyacrylonitrile Nanofibers and Its Application for the Photodegradation of Methyl Blue in Aqueous Medium, *Desalin. Water. Treat.*, **54(11)**: 3146-3151 (2015).

[20] Athar T., Synthesis and Characterization of Strontium Oxide Nanoparticles Via Wet Process, *Mater. Focus.*, **2(6)**: 450-453 (2013).

[21] Tamilisai R, Palanisamy P. N., Review on the Photocatalytic Degradation of Textile Dyes and Antibacterial Activities of Pure and Doped ZnO, *Int. J. Innov. Res.*, **8(3)**: 15-19 (2018).

[22] Prakash K., Senthil K.P., Latha P., Shanmugam R., Karuthapandian S., Dry Synthesis of Water Lily Flower Like SrO_2/g-C_3N_4 Nanohybrids for the Visible Light Induced Superior Photocatalytic Activity, *Materials Research Bulletin*, **93:** 112-122 (2017).

[23] Kılınc D., Sevim M., Eroğlu Z., Metin Ö., Karaca S., Strontium Oxide Modified Mesoporous Graphitic Carbon Nitride/Titanium Dioxide Nanocomposites (SrO-mpg-CN/TiO_2) as Efficient Heterojunction Photocatalysts for the Degradation of Tetracycline in Water, *Adv. Powder Technol.*, **32(8)**: 2743-2757 (2021).

[24] Yang M. Q., Zhang N. XU YJ., Synthesis of Fullerene-, Carbon Nanotube-, Andgraphene-TiO2 Nanocomposite Photocatalysts for Selective Oxidation: A Comparative Study, *ACS Appl. Mater. Interfaces*., **5(3)**: 1156-1164(2013).

[25] Nirmaladevi S., Palanisamy N., Preparation and Adsorptive Properties of Activated Carbon from Acacia Leucophloea Wood Sawdust Hydrochar by Zinc Chloride Activation, *Cellul. Chem. Technol.*, **53(9-10)**: 1029-1039 (2019).

[26] Nirmaladevi S., Palanisamy P.N., Adsorptive Behavior of Biochar and Zinc Chloride Activated Hydrochar Prepared from Acacia Leucophloea Wood Sawdust: Kinetic Equilibrium and Thermodynamic Studies, *Desalination Water Treat.* **209:** 170-181 (2021).

[27] Matos J., Chovelon J. M., Cordero T., Ferronato C., Influence of Surface Properties of Activated Carbon on Photocatalytic Activity of TiO2 in 4-chlorophenol Degradation, *The Open Environ. Eng. J.*, **2**: 21-29 (2009).

[28] Vijayalakshmi S., Anupriya P., Surya P., Vijayalakshmi C., Synthesis and Characterization of Strontia Nanoparticles, *Int. J. Pure. Appl. Math.*, **119(15)**: 1299-1305 (2018).

[29] Reddy C. V., Babu B., Shim J., Synthesis of Cr-Doped SnO_2 Quantum Dots and its Enhanced Photocatalytic Activity, *Mater. Sci. Eng. B.*, **223**: 131-142 (2017).

[30] Soltan W. B., Nasri S., Lassoued M. S., Ammar S., Structural, Optical Properties, Impedance Spectroscopy Studies and Electrical Conductivity of SnO_2 Nanoparticles Prepared by Polyol Method, *J. Mater. Sci-Mater. El.*, **28(9)**: 6649-6656 (2017).

[31] Rahman M. M., Hussain M. M., Asiri A. M., A Novel Approach Towards Hydrazine Sensor Development Using SrO· CNT Nanocomposites, *RSC Adv.*, **6(70)**: 65338-65348 (2016).

[32] Rahman Q. I., Ahmad M., Misra S. K., Lohani M., Effective Photocatalytic Degradation of Rhodamine B Dye by ZnO Nanoparticles, *Mater. Lett.*, **91**: 170-174 (2013).

[33] Ilyas M., Sadiq M., Liquid-Phase Aerobic Oxidation of Benzyl Alcohol Catalyzed by Pt/ZrO_2, Chemical Engineering & Technology: Industrial Chemistry-Plant Equipment-Process, *Eng.- Biotechnol.*, **30(10)**: 1391-1397 (2007).

[34] Makwana V. D, Son Y. C., Howell A. R., Suib S. L., The Role of Lattice Oxygen in Selective Benzyl Alcohol Oxidation Using OMS-2 Catalyst: A Kinetic and Isotope-Labeling Study, *J. Catal.*, **210(1)**: 46-52 (2002).

[35] Begum R., Naseem K., Ahmed E., Sharif A., Farooqi Z. H., Simultaneous Catalytic Reduction of Nitroarenes Using Silver Nanoparticles Fabricated in Poly (N-Isopropylacrylamide-acrylic acid-acrylamide) Microgels, *Colloids Surf, A Physicochem Eng Asp.*, **511:** 17-26 (2016).

[36] Farooqi Z. H., Sakhawat T., Khan S. R., Kanwal F., Usman M., Begum R., Synthesis, Characterization and Fabrication of Copper Nanoparticles in N-Isopropylacrylamide Based Co-Polymer Microgels for Degradation of P-Nitrophenol, *Mater. Sci.–Poland.*, **33**: 185-192 (2015).

[37] Begum R., Najeeb J., Ahmad G., Wu W., Irfan A., Al-Sehemi A.G., Farooqi Z.H., Synthesis and Characterization of poly (N-isopropylmethacrylamide-co-acrylic acid) Microgels for in Situ Fabrication and Stabilization of Silver Nanoparticles for Catalytic Reduction of O-Nitroaniline in Aqueous Medium, *React Funct Polym.*, **132:** 89-97 (2018).

[38] Saeed M., Siddique M., Ibrahim M., Akram N., Usman M., Aleem M.A., Baig A., Calotropis Gigantea Leaves Assisted Biosynthesis of ZnO and Ag@ ZnO Catalysts for Degradation of Rhodamine B Dye in Aqueous Medium, *Environ. Prog. Sustain. Energy.*, **39(4)**: 13408 (2020).

[39] Siddique M., Fayaz N., Saeed M., Synthesis, Characterization, Photocatalytic Activity and Gas Sensing Properties of Zinc Doped Manganese Oxide Nanoparticles, *Physica B: Condensed Matter.*, **602**: 412504 (2021).

[40] Naz F., Saeed K., Investigation of Photocatalytic Behavior of Undoped ZnO and Cr-doped ZnO Nanoparticles for the Degradation of Dye, *Inorg. Nano-Met. Chem.*, **51(1)**: 1-11 (2021).

[41] Pare B., Sarwan B., Jonnalagadda S. B., The Characteristics and Photocatalytic Activities of BiOCl as Highly Efficient Photocatalyst, *J. Mol. Struct.*, **1007**: 196-202 (2012).

[42] Nasser A.M.B., Muzafar A.K., Ioannis S.C, Hak Y K., Influence of Temperature on the Photodegradation Process Using Ag-Doped TiO_2 Nanostructures: Negative Impact with the Nanofibers, *J. Mol. Catal. A.*, **366**: 333–340. (2013)

[43] Kumar A., Mandal A., Dixit A. R, Das A. K., Performance Evaluation of Al_2O_3 Nano Powder Mixed Dielectric for Electric Discharge Machining of Inconel 825, *Mater. Manuf. Process.*, **33(9)**: 986-995 (2018).

[44] Gayathri K., Palanisamy N., Methylene Blue Adsorption onto an Eco-Friendly Modified Polyacrylamide/Graphite Composites: Investigation of Kinetics, Equilibrium, and Thermodynamic Studies, *Sep. Sci. Technol.*, **55(2)**: 266-277 (2020).

[45] Supriya S., Sathish S., Enhanced Photocatalytic Decolorization of Congo Red Dye with Surface-Modified Zinc Oxide using Copper(II)–amino Acid Complex, *Inorg. Nano-Metal Chem.*, **50(3)**: 100-109 (2020).

[46] Coleman H. M., Vimonses V., Leslie G., Amal R., Degradation of 1, 4-dioxane in Water Using TiO_2 Based Photocatalytic and H2O2/UV Processes, *J. Hazard. Mater.*, **146(3)**: 496-501 (2007).

[47] Cao G., "Nanostructures and Nanomaterials Synthesis, Properties and Applications", Imperial College Press, London, (2004).

[48] Rahimi R., Kerdari H., Rabbani M., Shafiee M., Synthesis, Characterization and Adsorbing Properties of Hollow Zn-Fe_2O_4 Nanospheres on Removal of Congo Red from Aqueous Solution, *Desalination*, **280**: 412–418 (2011).

[49] Hu C., Yu J C., Hao Z., Wong P K., Effect of Acidity and Inorganic Ions on the Photocatalytic Degradation of Different Azo Dyes, *Appl. catalysis B: Environmental*, **46(1)**: 35-47 (2003).

[50] Kermani M., Kakavandi B., Farzadkia M., Esrafili A., Jokandan S. F., Shahsavani A., Catalytic Ozonation of High Concentrations of Catechol Over TiO_2@ Fe_3O_4 Magnetic Core-Shell Nanocatalyst: Optimization, Toxicity and Degradation Pathway Studies, *J. Clean. Prod.*, **192**: 597-607 (2018).

[51] Moosavi S., Li R. Y. M, Lai C. W., Yusof Y., Gan S., Akbarzadeh O., Johan M. R., Methylene Blue Dye Photocatalytic Degradation over Synthesised Fe_3O_4/AC/TiO_2 Nano-Catalyst: Degradation and Reusability Studies, *Nanomaterials*, **10(12)**: 2360 (2020).